Effects of maleic anhydride grafted ethylene/vinyl acetate copolymer (EVA) on the properties of EVA/silica nanocomposites

Thai Hoang, Nguyen Thuy Chinh, Nguyen Thi Thu Trang, To Thi Xuan Hang, Dinh Thi Mai Thanh, Dang Viet Hung, Chang-Sik Ha, Maëlenn Aufray

Effects of Maleic Anhydride Grafted Ethylene/Vinyl Acetate Copolymer (EVA) on the Properties of EVA/Silica Nanocomposites

Thai Hoang*[,1], Nguyen Thuy Chinh[1], Nguyen Thi Thu Trang[1], To Thi Xuan Hang[1], Dinh Thi Mai Thanh[1], Dang Viet Hung[2], Chang-Sik Ha*[,3], and Maëlenn Aufray[4]

[1]Institute for Tropical Technology, Vietnam Academy of Science and Technology, 18 Hoang Quoc Viet, Cau Giay, Hanoi, Vietnam

[2]Hanoi University of Science and Technology, 1 Dai Co Viet, Hanoi, Vietnam

[3]Department of Polymer Science and Engineering, Pusan National University, Busan 609-735, Korea

[4]Inter-University Center for Materials Research and Engineering (CIRIMAT), 118 Narbonne, 31077 Toulouse Cedex 04, France

Abstract: Ternary nanocomposites based on ethylene/vinyl acetate copolymer (EVA), maleic anhydride-grafted EVA (EVAgMA), and nanosilica were prepared in a Haake Rheomixer. The structure of the EVA/EVAgMA/silica nanocomposites was characterized by Fourier transform infrared spectroscopy and field emission scanning electron microscopy. The blending sequence was found to have a significant effect on the microstructure of EVA/EVAgMA/silica nanocomposites and the dispersion behavior of the nanosilica in the EVA matrix. The tensile properties (tensile strength and elongation at break), thermal behavior, crystalline structure and weatherability of the nanocomposites were also studied. The results showed that the above properties of the nanocomposites were enhanced remarkably using 1 wt% EVAgMA.

Keywords: ethylene/vinyl acetate copolymer (EVA), nanosilica, nanocomposite, mechanical properties, thermal stability, weatherability.

Introduction

Ethylene/vinyl acetate copolymer (EVA) is used widely in electrical insulation, cable jacketing, encapsulation, packaging and corrosion protection, *etc*. The low cost and relatively good electrical and barrier properties of EVA have led to the continuous expansion of its applications, replacing other engineering plastics. On the other hand, the low tensile strength, thermal and UV stability of EVA have limited its applications in some fields.[1] To overcome these disadvantages, nanoparticles were added to this copolymer to improve the mechanical properties and thermal stability.[2-5]

The dispersion of silica nanoparticles (SNP) and the interfacial interaction between the SNP and polymer matrix play important roles to determine the properties of nanocomposites.[6-9] SNP exhibit high surface activity and large agglomeration due to the lack of coordinate atoms on the surfaces. Moreover, the poor compatibility between the SNP and EVA matrix leads to the formation of nanocomposites that cannot achieve the expected properties. Therefore, it is important to use suitable compatibilizers to improve the dispersibility of SNP in EVA, and the interfacial adhesion of SNP and EVA. Several studies related to SNP/polymer composites have focused on using amine and maleic anhydride - modified polypropylene (PP) as compatibilizers in PP/SNP nanocomposites to enhance the mechanical properties of the nanocomposites.[9-12] Hitherto, there has been little research on the use of a maleic anhydride modified EVA (EVAgMA) as a compatibilizer in EVA/SNP nanocomposites.

The main aim of this work was to examine the effects of EVAgMA on the rheological, mechanical properties, crystalline structure, thermal stability and weatherability of EVA/SNP nanocomposites. The interactions in the EVA/EVAgMA/SNP nanocomposites might include hydrogen bonding and dipole-dipole interactions between the carbonyl and C-O-C groups of MA in EVAgMA, as well as between the hydroxyl groups on the SNP surface and the carbonyl and C-O-C groups in EVA. These interactions might improve the dispersion of SNP in the EVA, which would enhance the properties of the EVA/silica nanocomposites.

Experimental

Ethylene/vinyl acetate copolymer (EVA) containing 10 wt% vinyl acetate (VAc) in granular form with a density of 0.93

*Corresponding Authors. E-mails: hoangth@itt.vast.vn or csha@pusan.ac.kr

g/cm^3 and melt flow index of 1.3 g/10 min/190 °C/2.16 kg was purchased from Hanhwa Co., Korea. Silica nanoparticles (SNP) with a purity of 99.8%, mean particle size of 12 nm, and specific surface area of approximately 175-225 m^2/g (BET) were obtained from Sigma-Aldrich Co. EVA grafted with 0.5 wt% maleic anhydride (MA) was purchased from Hanhwa Co., Korea.

Preparation of EVA/EVAgMA/SNP Nanocomposites (EMS). The nanocomposites containing 2 to 5 wt% SNP and 0 to 2 wt% EVAgMA were prepared by the melt mixing of EVA and SNP in a Haake Rheomixer (Germany) at a mixing temperature of 160 °C, mixing time of 5 min, and rotor speed of 50 rpm. After melt mixing, the nanocomposites were molded using a hot pressured machine (Toyoseiki Co.) at 160 °C at a 15 MPa pressure for 3 min to form samples with a thickness of approximately 1 mm. The samples examined are abbreviated in Table I. The EVAgMA and SNP contents were based on EVA by weight %.

Characterization. The relative melt viscosity, which is expressed as the torque values in the mixing process of EVA, SNP and EVAgMA, was recorded using Polylab 3.1 software connected to a Haake Rheomixer. The Fourier transform infrared (FTIR) spectra were recorded on a FTIR-Nexus infrared spectrometer using thin films of the samples prepared by compression molding in the range, 4000-400 cm^{-1}, at room temperature. The tensile properties, such as the tensile strength and elongation at break of EVA and EMS were measured on a Zwick Tensile 2.5 Machine according to the ASTM D638 standard. The morphology of the nanocomposites was analyzed by field emission scanning electron microscopy (FESEM, S-4800 Hitachi). X-Ray diffraction (XRD, Siemens D5000) was performed using CuK$_\alpha$ radiation (λ=0.154 nm) at 40 kV and 30 mA. The XRD data was collected between 5° and 60° 2θ at room temperature with a scanning speed of 0.7°/s and a step size of 0.03°. The thermal properties were measured on a DTG-60H and DSC-60 thermogravimetric analyzer (Shimadzu Co.) under an argon atmosphere from room temperature to 600 °C and at a heating rate of 10 °C/min. The relative crystallinity (χ_c) of the samples was calculated using the following equation:[10,13]

$$\chi_c = \Delta H_f \times 100 / \Delta H_f^*$$

where ΔH_f^* is the fusion enthalpy of the perfectly polyethylene crystal (298 J/g) and ΔH_f is the enthalpy of fusion of the samples.

The weatherability of the nanocomposites was analyzed using an accelerated weathering test on a UV-CON 327 (USA) according to the ASTM 793-91 (G32) method. Every cycle of the accelerated weathering test includes: 8 h of UV irradiation at 70 °C and 4 h of humidity condensation at 50 °C. The total testing time is 168 h (corresponding to 14 cycles). The tensile properties of the nanocomposites were determined before and after 6 and 14 cycles of the accelerated weathering test.

Results and Discussion

IR Spectra. Figure 1 presents the FTIR spectra of the SNP, EVA, E0M3S, and E1M3S nanocomposites. The spectrum of SNP showed the characteristic peaks, such as Si-O asymmetric and symmetric stretching vibrations (1110 and 794 cm^{-1}), Si-O bending vibrations (461 cm^{-1}) and Si-OH stretching vibrations (955 cm^{-1}), and the OH stretching and bending vibration (3448 and 1633 cm^{-1}, respectively).[14,15] The spectra of E0M3S and E1M3S clearly showed the char-

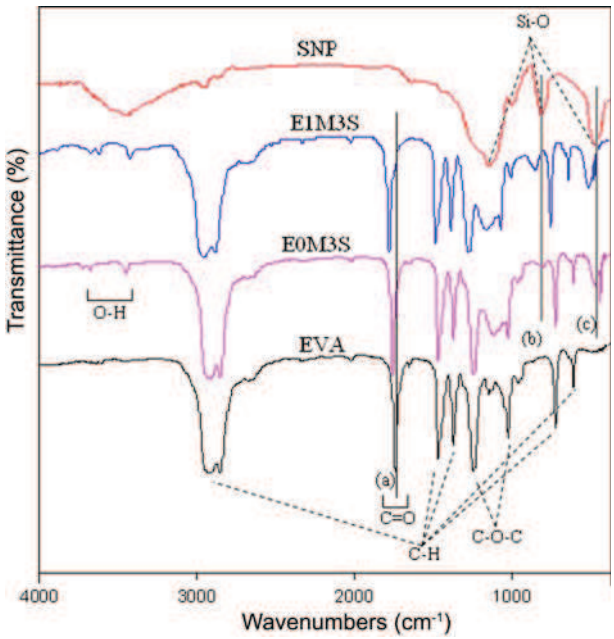

Figure 1. FTIR spectra of the EVA and EVA/SNP/EVAgMA nanocomposites.

Table I. Abbreviation of the EVA/EVAgMA/SNP Nanocomposite Samples

SNP Content (wt%) \ EVAgMA Content (wt%)	0	0.5	1	1.5	2
2	E0M2S	E0.5M2S	E1M2S	E1.5M2S	E2M2S
3	E0M3S	E0.5M3S	E1M3S	E1.5M3S	E2M3S
4	E0M4S	E0.5M4S	E1M4S	E1.5M4S	E2M4S
5	E0M5S	E0.5M5S	E1M5S	E1.5M5S	E2M5S

Table II. Characteristic Wavenumbers of the SNP, EVA, E0M3S, and E1M3S Samples

Samples	Wavenumbers (cm^{-1})								
	ν_{OH}	ν_{CH}	$\nu_{C=O}$	δ_{CH}	ν_{C-O}	ν_{Si-O}	ν_{Si-OH}	γ_{CH}	δ_{Si-O}
SNP	3448	2921 2847	-	-	-	1110 794	955	-	461
EVA	-	2924	1737	1456 1368	1242 1025			724	-
E0M3S	3500	2921 2852	1750	1463 1370	1241 1021	795		723	463
E1M3S	3612 3456	2925	1760	1457 1368	1244 1031	1127 804	-	724	482

acteristic peaks of EVA, such as the peaks at 1737 cm^{-1} for carbonyl and 1242 and 1025 cm^{-1} for C-O groups in the MA and acetate groups, as well as peaks at 2924, 1456, 1368, and 724 cm^{-1} due to the CH groups.[2,5] Some peaks observed at 795 and 804 cm^{-1} (Si-O-Si symmetric stretching vibration), and 463 and 482 cm^{-1} (Si-O-Si bending vibration) in the E0M3S and E1M3S spectra, respectively, were assigned to Si-O groups in nanosilica. A slight shift (6-23 cm^{-1}) was observed in the peaks of Si-O stretching and bending vibrations, and the C-O and C=O stretching vibrations, which was caused by the incorporation of EVAgMA in E1M3S (Table II). This suggests that the C=O and C-O-C groups of MA in EVAgMA interact with the hydroxyl groups on the SNP surface as well as carbonyl and C-O-C groups in EVA by hydrogen bonding and dipole-dipole interactions. Bikiaris *et al.* confirmed the aforementioned interactions between the carboxyl groups of PP-*g*-MA and the surface hydroxyl groups of SNP.[9]

Relative Melt Viscosity. Figure 2 shows the relative melt viscosity of the EVA/SNP nanocomposites, which is expressed by the torque in the melt mixing of EVA, SNP, and EVAgMA. The torque of the nanocomposites was higher than that of EVA. The internal friction generated in the mixing process

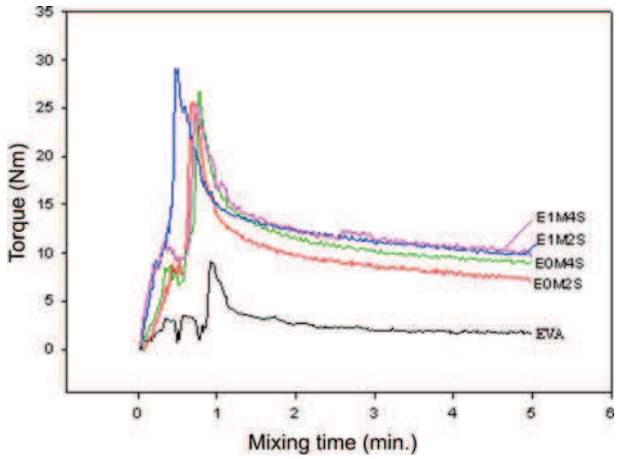

Figure 2. Torque of EVA and the nanocomposites during melt mixing.

between the SNP and EVA matrix causes an increase in torque. Normally, the torque of the nanocomposites depends on the SNP content and increase with increasing SNP content. In the presence of EVAgMA, the torque of the nanocomposites increased due to the fine SNP dispersion in EVA and the adhesion between the SNP and EVA. The interactions between EVAgMA and other components in the nanocomposites reduce the mobility of EVA chains. This leads to an increase in the torque of the E1M2S and E1M4S nanocomposites compared to EVA.[9] At the "equilibrium" state, the stable torque moment of EVA, E0M2S, E0M4S, E1M2S and E1M4S samples approached 1.8; 7.3; 9.2; 10.0 and 10.3 MPa, respectively. The stable torque moment of the nanocomposites using EVAgMA increased by between 12 and 37% compared to that of the nanocomposites without EVAgMA at the same SNP content.

Morphology. The interactions between the SNP and EVA matrix with and without EVAgMA in the EVA/SNP nanocomposites were evaluated by FESEM (Figure 3). FESEM of the cryo-fractured surface of the nanocomposites without EVAgMA (Figure 3(a)-(d)) indicated an irregular dispersion of SNP in the EVA matrix. The SNP agglomerated to form large clusters in the EVA matrix, from 100 nm-2 μm, which causes a decrease in the mechanical properties of the nanocomposites presented in Tensile Properties section.

For nanocomposites containing EVAgMA, the particle agglomerate sizes were less than 200 nm (Figure 3(e)-(h)). This suggests that the SNP are well dispersed and adhered to EVA due to the presence of EVAgMA. The decrease in particle agglomerate size can explain the increase in the mechanical properties and thermal stability of the nanocomposites containing EVAgMA.[9,15]

Tensile Properties. Figure 4 shows the tensile strength of the EVA/SNP nanocomposites. The tensile strength of the nanocomposites at different EVAgMA and SNP contents was higher than that of the neat EVA (17.3 MPa). SNP can enhance the tensile strength of the nanocomposites due to interactions between the nanoparticles and EVA matrix at the molecular level.[7] The tensile strength of the EVA/SNP nanocomposites with EVAgMA was higher than that of the

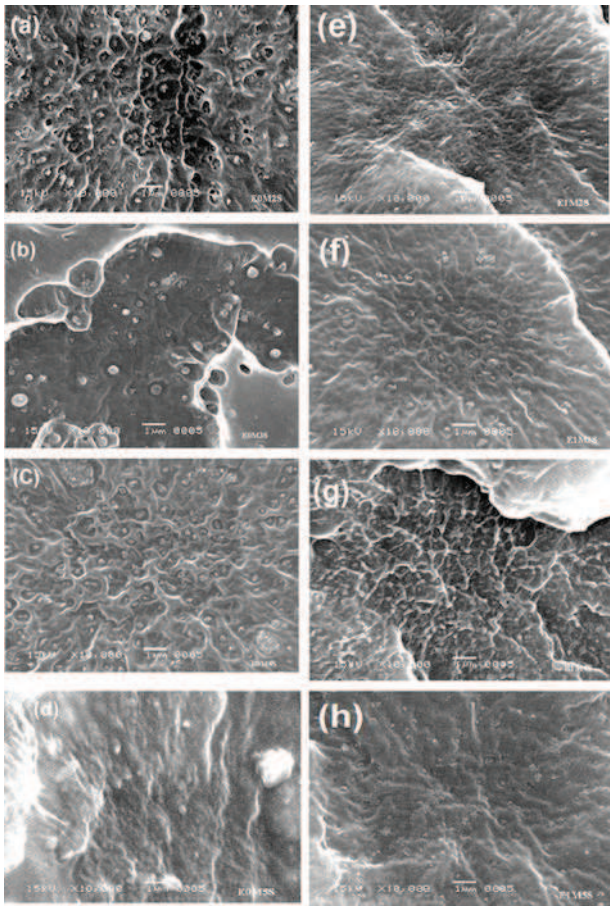

Figure 3. SEM images of the cryo-fractured surface the EVA/SNP nanocomposites; (a) E0M2S; (b) E0M3S; (c) E0M4S; (d) E0M5S; (e) E1M2S; (f) E1M3S; (g) E1M4S; (h) E1M5S.

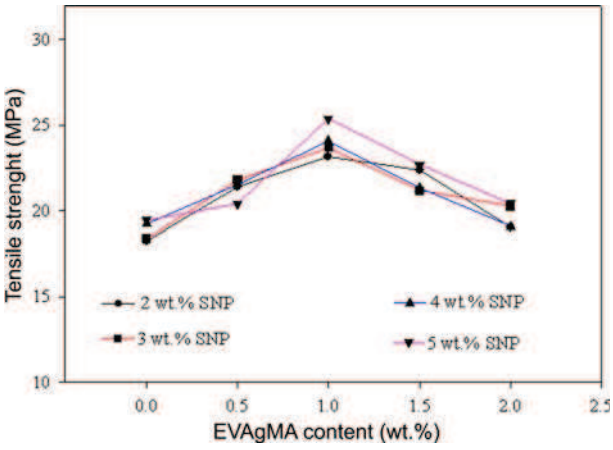

Figure 4. Effect of the EVAgMA and SNP content on the tensile strength of the EVA/SNP nanocomposites: 2 wt% SNP: (-•-), 3 wt% SNP: (-■-), 4 wt% SNP: (-▲-), 5 wt% SNP: (-▼-).

EVA/SNP nanocomposites without EVAgMA. The maximum tensile strength of the nanocomposites was observed at 1 wt% EVAgMA. Similar results were also obtained in the poly(ethylene 2,6-naphthalate)/silica nanocomposites,[6] PP/SiO_2 nanocomposites[9,12] and poly(ethyl methacrylate-*co*-hydroxyethyl acrylate) (P(EMA-*co*-HEA))/silica nanocomposites.[11] Presumably, EVAgMA localized at the interface between the SNP and matrix polymer is responsible for the enhanced mechanical properties of the nanocomposites. The interactions and good dispersion between EVA and SNP can improve the mechanical properties of the nanocomposites. On the other hand, the tensile strength showed a decrease tendency when the EVAgMA content in the nanocomposites exceeded 1 wt%.

Similarly, at a constant EVAgMA content (1 wt%), the tensile strength of the nanocomposites increased with increasing SNP content. For example, at 2, 3, 4, and 5 wt% of SNP, the maximum tensile strength of the nanocomposites using 1 wt% EVAgMA was 23.2, 23.7, 24.1, and 25.4 MPa, respectively, showing a corresponding increase of 27.5, 28.8, 25.5, and 30.1%, compared to the samples without EVAgMA. This can be explained by the role of EVAgMA in inducing inter-molecular interactions between EVA and SNP leading to improved compatibility of the EVA and SNP phases. At an EVAgMA content less than 1 wt%, the amount of EVAgMA might not be sufficient to induce inter-molecular interactions between EVA and SNP. Therefore, the change in the tensile strength of the nanocomposites was not great. In contrast, the agglomeration of EVAgMA can occur when EVAgMA content exceeds 1 wt%, leading to an irregular dispersion of SNP into the EVA matrix. Therefore, the tensile strength of the nanocomposites can decrease.

Figure 5 shows the elongation at break of the nanocomposites with various EVAgMA and SNP contents. The elongation at break of EVA/SNP nanocomposites decreased with increasing SNP content in the EVA matrix because the hard and rigid SNP act as stress concentrators, providing less ductility to the nanocomposites. In particular, when the SNP content was increased to 4-5 wt%, the size of the

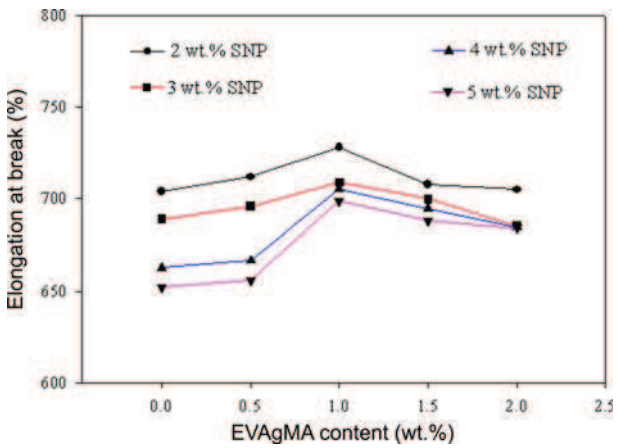

Figure 5. Effect of the EVAgMA and SNP content on the elongation at break of the EVA/SNP nanocomposites: 2 wt% SNP: (-•-), 3 wt% SNP: (-■-), 4 wt% SNP: (-▲-), 5 wt% SNP: (-▼-).

Table III. DSC Data of EVA and the EVA/SNP Nanocomposites[a]

Samples	$T_{m\text{-}m}$ (°C)	ΔH_f (J/g)	χ_c (%)
EVA	96.1	67.7	22.7
E0M2S	96.1	61.5	20.6
E0M3S	97.0	64.1	21.5
E0M4S	96.1	62.6	21.0
E0M5S	96.2	63.3	21.2
E1M2S	95.7	55.6	18.7
E1M3S	97.4	66.5	22.3
E1M4S	95.9	59.5	20.0
E1M5S	96.0	55.3	18.6

[a] $T_{m\text{-}m}$: melting temperature; ΔH_f: enthalpy of fusion; χ_c: relative crystallinity.

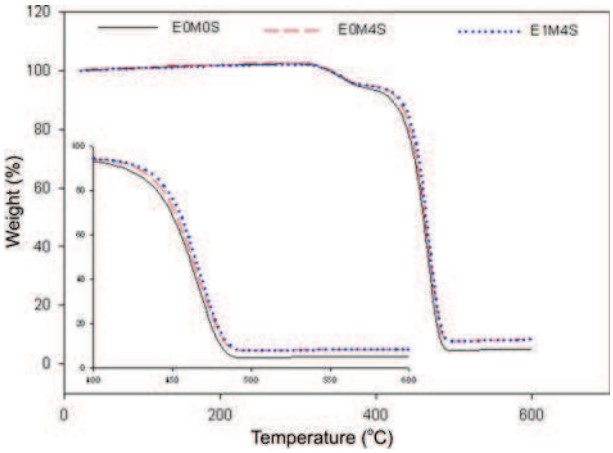

Figure 6. TGA curves of EVA, E0M4S and E1M4S.

agglomerated particles increased, indicating a higher stress concentration, more extensive cavitation and faster breaking.[9,11,12] The elongation at break of the EVA/SNP nanocomposites with EVAgMA was higher than that of the nanocomposites without EVAgMA and reached the maximum at 1 wt%. Using a constant EVAgMA content (1 wt%), the maximum elongation at break of the nanocomposites decreased with increasing SNP content.

Thermal Properties and Thermal Stability. The melting temperature of all EVA/silica nanocomposites with and without EVAgMA was observed at approximately 96 °C with marginal differences, as shown in Table III. On the other hand, when adding SNP and EVAgMA into EVA and the nanocomposites, the chain segments possessing vinyl acetate (VAc) units in the amorphous and ethylene chain segments in the secondary crystallization region could re-arrange.[1,10,13,16] This might explain the slight decrease in overall crystallinity (χ_c %).

Figure 6 and Table IV respectively show TGA curves and the TG characteristic data of EVA and the EVA/SNP nanocomposites. The weight loss of all samples is related to two steps of EVA degradation corresponding two temperatures with the maximal degradation rate (T_{p1}, T_{p2}). The first stage was complete at approximately 400 °C, involving mainly autocatalytic deacetylation in the VAc moieties. The second stage is chain scission of the residual main polyethylene chains within an interval of 405-500 °C.[1,10,17] When adding SNP to EVA, the weight loss in the 1st stage (ΔW_1) of the nanocomposites was lower than that of EVA, and the onset temperatures ($T_{On\text{-}d}$), which are the temperatures corresponding to 10%, 20% and 50% weight loss (T_{10}, T_{20}, and T_{50}), were higher than those of EVA. This can be explained by the high thermal stability of SNP when the SNP are dispersed regularly in the EVA matrix, which have a protective agent and barrier effect for EVA at high temperature. Therefore, the thermal stability

Table IV. TG and DTG Results of EVA and the EVA/SNP Nanocomposites[a]

Samples	TG					DTG	
	$T_{On\text{-}d}$ (°C)	T_{10} (°C)	T_{20} (°C)	T_{50} (°C)	ΔW_1 (%)	T_{p1} (°C)	T_{p2} (°C)
EVA	348	419	439	460	7.78	351	458
E0M2S	349	424	443	462	7.58	355	463
E0M3S	350	425	443	462	7.51	370	467
E0M4S	360	428	444	463	7.42	360	466
E0M5S	356	427	446	464	7.35	348	471
E1M2S	358	425	445	462	7.47	354	470
E1M3S	361	428	445	463	7.40	352	470
E1M4S	359	429	447	464	7.04	358	466
E1M5S	353	423	443	463	7.68	356	471

[a] $T_{On\text{-}d}$: the onset temperature of weight loss (weight loss at about 3%); T_{10}: temperature corresponding to 10% weight loss; T_{20}: temperature corresponding to 20% weight loss; T_{50}: temperature corresponding to 50% weight loss; ΔW_1: weight loss in the first stage; T_{p1}: temperature of the maximal degradation rate of stage 1; T_{p2}: temperature of the maximal degradation rate of stage 2.

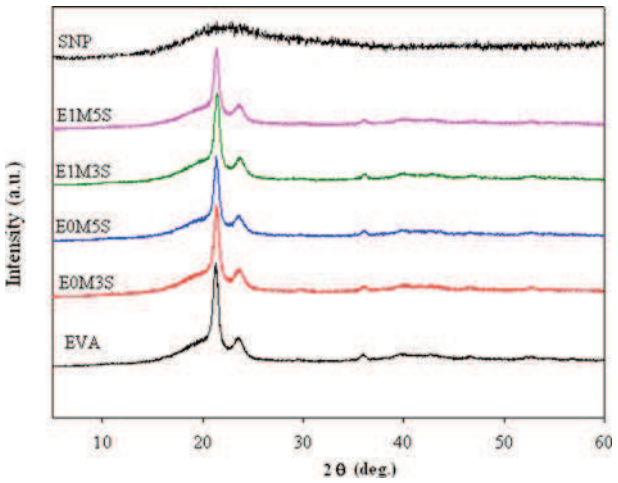

Figure 7. XRD patterns of the SNP, EVA and EVA/SNP nanocomposites with and without 1 wt% EVAgMA.

Table V. Diffraction Angle (2θ), *d*-Spacing (*d*), and Lateral Crystal Size (*L*) of SNP, EVA and EVA/SNP Nanocomposites with and without 1 wt% EVAgMA, Obtained from XRD

Sample	$2\theta_{110}$ (°)	d_{110} (nm)	d_{200} (nm)	L_{110} (nm)
EVA	21.26	4.176	3.774	0.511
E0M2S	21.27	4.175	3.778	0.506
E0M3S	21.33	4.162	3.767	0.505
E0M4S	21.37	4.156	3.762	0.483
E0M5S	21.32	4.165	3.774	0.505
E1M2S	21.32	4.165	3.765	0.480
E1M3S	21.38	4.153	3.752	0.491
E1M4S	21.20	4.187	3.777	0.510
E1M5S	21.32	4.165	3.777	0.508

of EVA increases in the presence of SNP.[8,10]

The $T_{On\text{-}d}$, T_{10}, T_{20}, and T_{50} were shifted to higher temperatures, in range of 2-10 °C, due to the presence of EVAgMA in the EVA/SNP nanocomposites (Table IV). This suggests that EVAgMA can enhance the thermal stability of the EVA/SNP nanocomposites. The EVA/SNP nanocomposites containing 1 wt% EVAgMA have lower ΔW_1 values and higher T_{p1} and T_{p2} than those of the nanocomposites without EVAgMA. The peak positions of T_{p1} and T_{p2} (DTG data not shown) might change with different EVAgMA content.[10]

X-Ray Diffraction. Figure 7 shows XRD patterns of SNP, EVA and different EVA/SNP nanocomposites, showing that SNP is amorphous. The broad peak might be due to the small size and incomplete inner structure of the particles.[18]

EVA possesses both crystalline and amorphous regions. Therefore, two sharp XRD peaks at 21.26° 2θ (110 plane) and 23.60° 2θ (200 plane) were observed for EVA. Accordingly, the XRD patterns of all EVA containing nanocomposites showed an intense peak at approximately 21° 2θ, which corresponds to the crystalline regions, whereas the weak peak approximately 23° 2θ was assigned to the amorphous regions in EVA. The EVA crystalline or amorphous structural state appears to depend on the fraction of components in the nanocomposites. For the nanocomposites, however, the positions of the XRD peaks did not shift significantly compared to those of neat EVA. This suggests that the crystalline structure of EVA remains unchanged upon the addition of different SNP and EVAgMA contents during preparation of the EVA/SNP nanocomposites. No additional peaks were observed, which suggests no third phase in the nanocomposites.[19]

The relative intensity of these peaks decreased in all nanocomposites, corresponding to a decrease in their overall crystallinity, as reported elsewhere.[2,13,18] The change in the relative intensity of the peaks in the nanocomposites might be due to the crystal alignment during the preparation process. Interestingly, the relative intensity of the diffraction peaks of the E1M3S samples was higher than the other samples, indicating an enhancement of diffuse amorphous scattering and an increase in overall crystallinity. This is in accordance with the DSC results reported above.

Table V lists the characteristic Bragg angles (2θ) and corresponding *d*-spacing (*d*) determined from the Bragg's equation (eq. (9) in ref. 13), as well as the lateral crystal size calculated using the Scherrer's equation (eq. (10) in ref. 13) based on the XRD patterns. The addition of SNP and EVAgMA to EVA can reduce slightly the *d*-spacing and crystal domain sizes of EVA. The result might also be due to the role of EVAgMA in enhancing the compatibility between the SNP and EVA matrix. The decrease in the bulk crystallization rate and crystal domain sizes might result in a lower degree of crystallinity in EVA.[18]

Weatherability. Figure 8 shows the FTIR spectra of EVA and the EVA/SNP nanocomposites before and after the

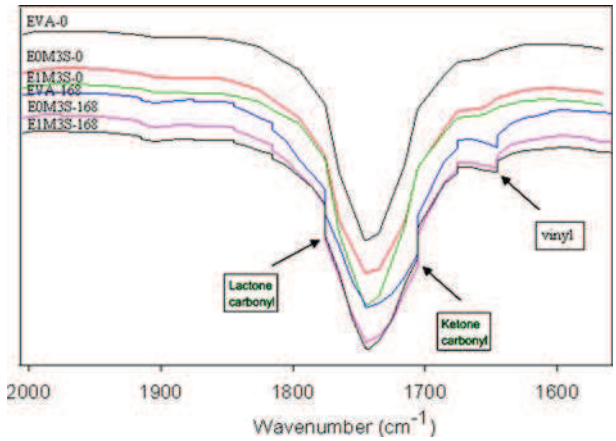

Figure 8. FTIR spectra in the range 2000-1550 cm^{-1} of EVA and the nanocomposites after the 168 h accelerated weathering test.

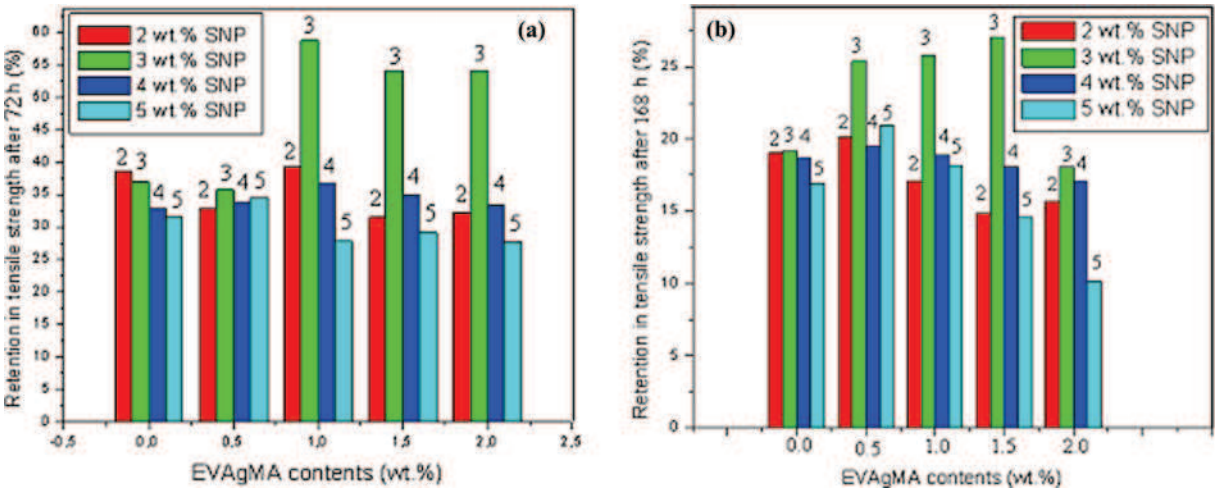

Figure 9. Retention of the tensile strength after the 72 h (a) and 168 h (b) accelerated weathering test; 2, 3, 4, 5: 2, 3, 4, 5 wt% SNP.

accelerated weathering tests. The change in the characteristic peaks of the main functional groups in EVA and the nanocomposites is related to the UV degradation of EVA initiated by the release of acetic acid from EVA. For the tested samples, the growth in the absorption shoulder at approximately 1715 cm^{-1} was assigned to the carbonyl C=O stretching vibration in the rapidly forming ketone structure. The absorption band at approximately 1630 cm^{-1} was assigned to the C=C stretching mode. This might be obtained during the acetaldehyde evolution process in the Norrish III photolysis reaction (Scheme I in ref. 10), or it might be obtained during the Norrish II reaction procedures forming vinyl, vinylidene and *trans*-vinylene unsaturated groups (Schemes I and II, IV in ref. 20 and ref. 10). The emergence of a new carbonyl shoulder vibration at 1780 cm^{-1} was attributed mainly to lactone formation, as reported by Allen.[21]

A comparison of the non-polar ethylene chain segments showed that the VAc units are more vulnerable to heat, oxygen and UV light radiation, which can form reactive radicals or unstable hydro peroxide easily, and facilitate further irreversible chemical reactions. Along with the accumulation of unstable structures and oxygen penetration, degradation of the molecules extends from the surface to the entire sample (see Figure 10 later).

Figure 9 shows the retention of the tensile strength of the nanocomposites after the 72 and 168 h accelerated weathering test. The addition of EVAgMA and SNP to EVA led to an increase in the percentage retention of the tensile strength of

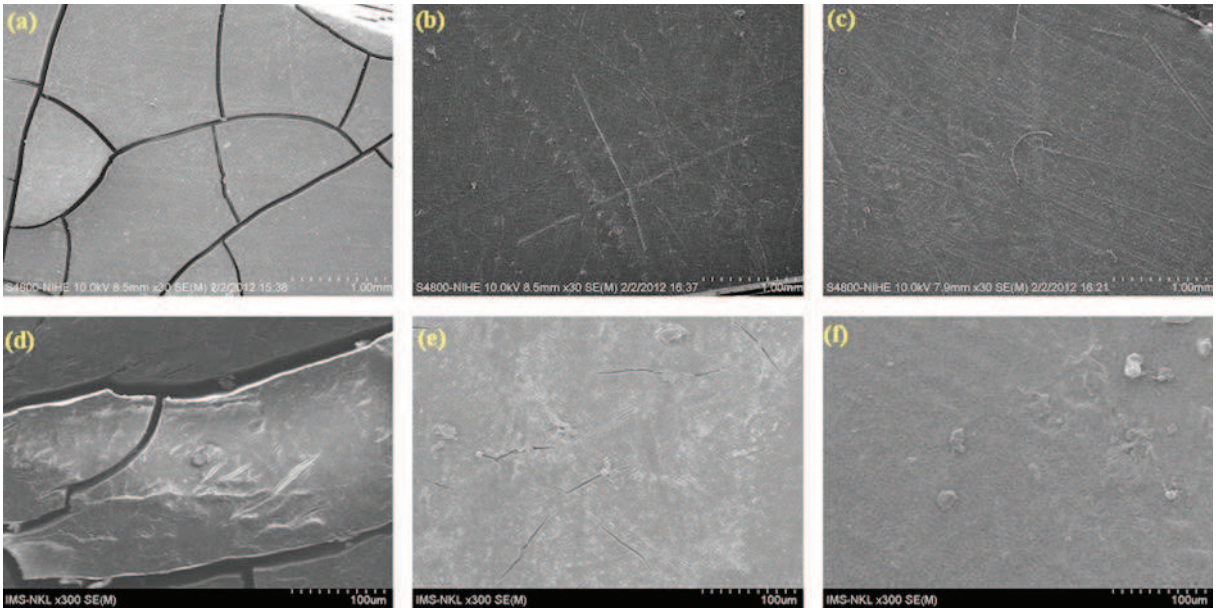

Figure 10. SEM images of the nanocomposites after the accelerated weathering test; (a) EVA; (b) E0M3S; (c) E1M3S (magnification 100 times); (d) EVA; (e) E0M3S; (f) E1M3S (magnification 10,000 times).

the nanocomposites compared to that of neat EVA (24.3% after 72 h and 10.5% after 168 h compared to that of neat EVA before testing (17.3 MPa)).

At low EVAgMA contents (0-0.5 wt%), the retention in the tensile strength of all nanocomposites was similar. The retention of the tensile strength of the nanocomposites using EVAgMA tended to decrease except for the nanocomposites containing 3 wt% SNP. The increase in the accelerated weathering test time resulted in a decrease in retention in the tensile strength of all nanocomposites. This can be explained by a rearrangement in the crystalline region leading to cracks on the surface of the material (Figure 10). The chain scission gives rise to a stress concentration and crack propagation in the material, which leads to a further decrease in the mechanical properties.[10,22] The nanocomposites containing 3 wt% SNP at all EVAgMA contents showed the highest retention in tensile strength due to the highest crystalline percentage, as shown in Table III.

Figure 10 presents FESEM images of the surface of the nanocomposites after the 168 h accelerated weathering test. The EVA film showed large, deep and linear cracks on both the surface and deep inside of the sample (Figure 10(a) and (d)). The E0M3S and E1M3S samples, however, showed some niches on the surface (Figure 10(b) and (e), Figure 10(c) and (f)). This suggests that the SNP can limit the decomposition of the EVA in the presence of UV radiation. In addition, the E1M3S sample showed no niches, whereas the E0M3S sample showed only a few small niches. Therefore, the E1M3S sample has better weatherability than that the E0M3S and EVA samples (Figure 9).

Conclusions

This study examined the effects of the addition of EVAgMA on the rheological, mechanical properties, thermal stability, crystalline structure and weatherability of the EVA/SNP nanocomposites. The use of EVAgMA produced remarkable enhancement in the relative melt viscosity, tensile strength, elongation at break, thermal stability and weatherability of the EVA/SNP nanocomposites. The overall crystallinity of EVA decreased when SNP and EVAgMA were added. Furthermore, the SNP dispersed evenly into EVA in the presence of EVAgMA might act a good UV stabilizer for EVA. In particular, the weatherability of the EVA/SNP nanocomposites was clearly improved using only 1-1.5 wt% EVAgMA and 3 wt% SNP.

Acknowledgments. The authors would like to thank the National Foundation for Science and Technology Development of Vietnam (NAFOSTED, 104.04-2010.02) and Vietnam Academy of Science and Technology (VAST-CNRS of France Project of Corrosion and Protection of Materials in period 2011-2012) for the financial support. CSH also thanks to the National Research Foundation of Korea (NRF) Grant funded by the Ministry of Science, ICT & Future Planning, Korea (Acceleration Research Program (2013) and Pioneer Research Center Program (2013)).

References

(1) B. Wang, X. Wang, Y. Shi, G. Tang, Q. Tang, L. Song, and Y. Hu, *Radiat. Phys. Chem.*, **81**, 308 (2012).
(2) M. Sadeghi, G. Khanbabaei, A. H. S. Dehaghani, M. Sadeghi, M. A. Aravanda, M. Akbarzadec, and S. Khatti, *J. Memb. Sci.*, **322**, 423 (2008).
(3) P. Cassagnau, *Polymer*, **44**, 2455 (2008).
(4) S. Hui, T. K. Chaki, and S. Chattopadhyay, *Polym. Eng. Sci.*, **50**, 730 (2010).
(5) J. Kruenate, R. Tongpool, and P. Kongrat, *J. Metastable Nanocryst. Mater.*, **23**, 227 (2005).
(6) S. H. Ahn, S. H. Kim, B. C. Kim, K. B. Shim, and B. G. Cho, *Macromol. Res.*, **12**, 293 (2004) .
(7) S. H. Ahn, J. T. Park, J. H. Kim, Y. Ko, and S. U. Hong, *Macromol. Res.*, **19**, 1195 (2011).
(8) E. S. Jang, S. B. Khan, J. Seo, K. Akhtar, J. Choi, K. I. Kim, and H. Han, *Macromol. Res.*, **19**, 1006 (2011).
(9) D. N. Bikiaris, A. Vassiliou, E. Pavlidou, and G. P. Karayannidis, *Eur. Polym. J.*, **41**, 1965 (2005).
(10) J. Jin, S. Chen, and J. Zhang, *Polym. Degrad. Stab.*, **95**, 725 (2010).
(11) A. Vallés-Lluch, G. G. Ferrer, and M. M. Pradas, *Eur. Polym. J.*, **46**, 910 (2010).
(12) J. H. Chen, M. Z. Rong, W. H. Ruan, and M. Q. Zhang, *Compos. Sci. Technol.*, **69**, 252 (2009).
(13) A. Shahin, S. Alireza, K. Mohammadreza, E. Alireza, P. Mohammadhadi, S. Mazinani, and A. Mehdi, *Mater. Des.*, **33**, 273 (2012).
(14) P. Liu, Q. Wang, X. Li, and C. Zhang, *Colloids Surf. A: Physicochem. Eng. Asp.*, **334**, 112 (2009).
(15) H. J. Zhou, M. Z. Rong, M. Q. Zhang, and K. Friedrich, *J. Mater. Sci*., **41**, 5767 (2006).
(16) F. Laoutid, L. Ferry, E. Leroy, and J. M. L. Cuesta, *Polym. Degrad. Stab.*, **91**, 2140 (2006).
(17) C. Nyambo, E. Kandare, and A. W. Charles, *Polym. Degrad. Stab.*, **94**, 513 (2009).
(18) M. Jafarzadeh, I. A. Rahman, and C. S. Sipaut, *Ceram. Int.*, **36**, 333 (2010).
(19) M. Madani, *Bull. Mater. Sci.*, **33**, 65 (2010).
(20) R. Scaffaro, L. Botta, and G. Gallo, *Polym. Degrad. Stab.*, **97**, 653 (2012).
(21) N. S. Allen, M. Edge, M. Rodriguez, C. M. Liauw, and E. Fontan, *Polym. Degrad. Stab.*, **68**, 363 (2000).
(22) G. Oreski and G. M. Wallner, *Solar Energy*, **83**, 1040 (2009).